



BI-DIRECTIONAL HOLOGRAPHIC LENS FOR SIMULTANEOUS CONTROL OF REFLECTED AND TRANSMITTED ULTRASONIC FIELDS

Eric Ballestero^{1*} Josep Rodríguez-Sendra² Jean-Philippe Groby¹
 Vicent Romero-García³ Noé Jiménez²

¹ Laboratoire d'Acoustique de l'Université du Mans, LAUM - UMR 6613 CNRS, Le Mans Université, France

² Instituto de Instrumentación para Imagen Molecular, Consejo Superior de Investigaciones Científicas (CSIC), Universitat Politècnica de València, València, Spain.

³ Instituto Universitario de Matemática Pura y Aplicada (IUMPA), Departamento de Matemática Aplicada, Universitat Politècnica de València, València, Spain.

ABSTRACT

Holographic lenses enable phase profile storage in monolithic elements for wavefield manipulation, benefiting beamforming and imaging applications. In ultrasounds, precise control over both reflected and transmitted fields is highly sought after, particularly in non-invasive biomedical contexts. However, the simultaneous control of both fields remains largely unexplored in ultrasounds, despite its potential in optics. In this study, we introduce a bi-directional asymmetric ultrasonic lens that operates concurrently in transmission and reflection, offering spatial phase encoding for both directions. As an illustrative example, we demonstrate a lens that exhibits bidirectional Lambertian scattering, resulting in a quasi-omnidirectional scattering pattern for both reflected and transmitted fields. This serves as a fundamental framework for further investigations into a wide range of reflected and transmitted wavefields. By expanding this work on simultaneous wavefields, new possibilities can emerge for ultrasound applications, including improved beam control, cancellation of specular reflections, and exploration of novel wavefield manipulation techniques.

*Corresponding author: [eric.ballestero\[a\]univ-lemans.fr](mailto:eric.ballestero[a]univ-lemans.fr).

Copyright: ©2023 Eric Ballestero et al. This is an open-access article distributed under the terms of the Creative Commons Attribution 3.0 Unported License, which permits unrestricted use, distribution, and reproduction in any medium, provided the original author and source are credited.

Keywords: *ultrasounds, holograms, scattering, multi-objective optimisation, biomedical imaging.*

1. INTRODUCTION

Biomedical applications encompass a great part of ultrasound research, mostly for medical imaging [1] and non-invasive therapy [2]. It can enhance visualization of organs for precise targeting using techniques like ultrasensitive Doppler imaging (uDoppler) [3] or ultrasound localisation microscopy (ULM) [4]. Many non-invasive treatments employ localized ultrasonic fields, such as beam steering/focusing [5] combined with High Intensity Focused Ultrasounds (HIFU) [6] for heat-induced tissue ablation. For such tasks, acoustic holograms/lenses [7, 8], offer cost-effective alternatives for enabling control of ultrasonic wavefields over complex multi-transducer setups [9]. A such, they can help improve spatial imaging resolution and facilitate customized therapy by encoding the desired wavefronts into materials with different local propagation speeds [10]. The resulting scattered wavefield of the surface phase distribution is then determined by the well-known spatial Fourier transform. Inspired by concert hall acoustic diffusers [11, 12], such ultrasonic diffusers can help reduce specularity and more generally help distribute wavefields in any desired way. In this work, we present a bi-directional asymmetric ultrasonic lens that simultaneously controls reflected and transmitted wavefields by compressing two scattering patterns on each of

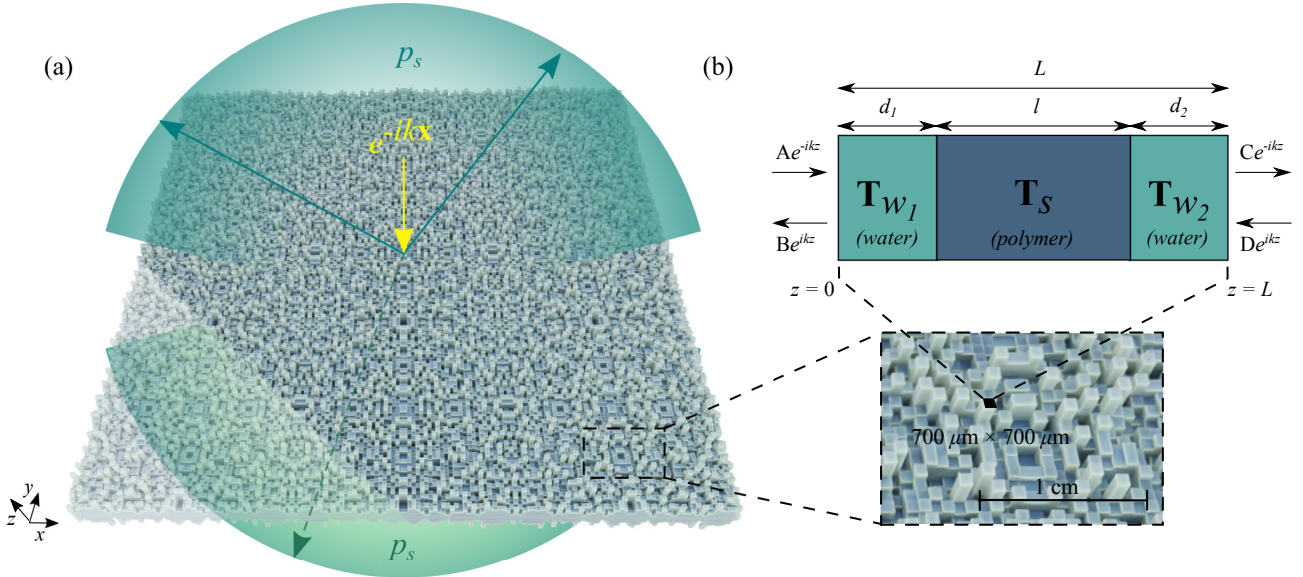


Figure 1. (a) Artistic impression of a $10 \times 10 \times 1$ cm ultrasonic bi-directional diffusing lens with uniform scattering profiles for each direction; reflection in blue, transmission in green. (c) Representative 1D Scattering Matrix diagram of a block of total length L composed of a polymer element and an exterior water medium.

its faces, instead of the typical one in transmission. The lens thus serves as a bi-directional diffusing lens, similar to optical diffusers, and enables beam directivity selection, where it can reduce unwanted reflections during ultrasound-guided procedures.

2. THEORY & PHASE-SPACE OPTIMIZATION

We examine a polymer-based ultrasonic lens operating at a frequency of 1.1 MHz and surrounded by water. The lens consists of multiple monolithic blocks which will help adapt the phase profile at each face of the diffuser. A visual representation of a sample configuration is illustrated in Fig. 1(a).

On the one hand, we consider first a 1D problem for each constituting block of the lens, where the sound pressures, p , and normal particle velocities, v_z , at the beginning ($z = 0$) and at the end of the panel ($z = L$) can be modelled by means of the Transfer Matrix Method (TMM) [13]. Assuming plane wave propagation in the system, the transfer matrix \mathbf{T} can be derived and the reflection and transmission coefficients calculated. Such approximation can be made due to the low difference in impedance between the water and polymer media, with a

polymer-to-water impedance ratio $Z_p/Z_w = 1.67$. This system illustrated in Fig. 1(b) can thus be written as

$$\begin{bmatrix} p \\ v_z \end{bmatrix}_{z=0} = \mathbf{T} \begin{bmatrix} p \\ v_z \end{bmatrix}_{z=L} = \begin{bmatrix} T_{11} & T_{12} \\ T_{21} & T_{22} \end{bmatrix} \begin{bmatrix} p \\ v_z \end{bmatrix}_{z=L}, \quad (1)$$

where \mathbf{T} is given by the product of the transfer matrices of the different media constituting each block cell, i.e.,

$$\mathbf{T} = \mathbf{T}_{w1} \mathbf{T}_p \mathbf{T}_{w2}, \quad (2)$$

where \mathbf{T}_w and \mathbf{T}_p are the transfer matrices of the water and polymer media, respectively, which take here the form of homogeneous and isotropic media slabs with complex effective propagation parameters defined by the nature of the media [13].

On the other hand, the scattering matrix, \mathbf{S} , relates the amplitudes of the incoming waves to those of the outgoing waves. Thus the relation between the amplitudes of the waves as shown in Fig. 1(b), is given by the \mathbf{S} -matrix as

$$\begin{bmatrix} C \\ B \end{bmatrix} = \mathbf{S} \begin{bmatrix} A \\ D \end{bmatrix} = \begin{bmatrix} T^- & R^+ \\ R^- & T^+ \end{bmatrix} \begin{bmatrix} A \\ D \end{bmatrix}, \quad (3)$$

where the elements of the \mathbf{S} -matrix give directly the transmission (T^- and T^+) and reflection (R^- and R^+)

coefficients for a system excited from each side of the structure. The superscripts (+, -) denote the direction of incidence, i.e., from the positive and negative z -axis respectively. The \mathbf{S} -matrix is widely used in wave physics to characterize and interpret wave scattering.

Considering a transmission problem and the system to be asymmetric (i.e., no mirror symmetry with respect to $z = L/2$, implying $R^+ \neq R^-$) and reciprocal (i.e., linear and time-invariant system, implying $T^+ = T^-$), the transmission and reflection coefficients, T and R^\pm , can be expressed from both sides in function of the transfer matrix elements outlined in Eq. 1, written as [13]

$$T = \frac{2}{T_{11} + T_{12}/Z_0 + T_{21}Z_0 + T_{22}}, \quad (4)$$

$$R^- = \frac{T_{11} + T_{12}/Z_0 - T_{21}Z_0 - T_{22}}{T_{11} + T_{12}/Z_0 + T_{21}Z_0 + T_{22}}, \quad (5)$$

$$R^+ = \frac{-T_{11} + T_{12}/Z_0 - T_{21}Z_0 + T_{22}}{T_{11} + T_{12}/Z_0 + T_{21}Z_0 + T_{22}}. \quad (6)$$

Following Fraunhofer's diffraction theory, the far-field pressure distribution at normal incidence, $p_s(\theta, \phi)$, of a radiating rectangular surface with a spatially dependent phase distribution coefficient, $\xi(x, y)$, of size $2a$ and $2b$ in the x and y directions respectively, can be calculated by the integral [14]

$$p_s(\theta, \phi) = \iint_S \xi(x, y) e^{ik(x \sin \phi \sin \theta + y \sin \phi \cos \theta)} dS, \quad (7)$$

where θ and ϕ are the azimuthal and elevational angles, respectively. Here $\xi(x, y)$ can be replaced by either phase-distribution $T(x, y)$ or $R^\pm(x, y)$ for obtaining the scattered pressure field in transmission or reflection.

Before designing a phase-distributed lens, an important step is to determine the appropriate lengths of polymer l within a total length L , surrounded by water layers d_1 and d_2 , to achieve desired combinations of phase angles (Φ^R, Φ^T) for reflected and transmitted wavefronts. For instance, achieving $\Phi^R = -\pi$ rad in reflection and $\Phi^T = 0$ rad in transmission at the same (x, y) location. This can be accomplished by plotting the phases of the reflection and transmission coefficients in a phase-space matrix, enabling the identification of potential block lengths to replicate any desired phase distribution on both sides of the lens.

To determine the set of lengths that correspond to specific phase combinations (Φ^R, Φ^T) within the phase-space, a multi-objective minimization algorithm, such as a genetic algorithm, can be employed. This algorithm optimizes one criterion while considering the other as a function of the former. As such, a range of viable solutions (i.e., polymer material lengths l with varying water gaps d_1 and d_2 on either side) can be obtained to achieve the desired phase combinations (Φ^R, Φ^T) . This set of solutions that satisfy the optimization objectives in such problems are often referred to as a Pareto front. The present multi-objective minimization algorithm aims to minimize cost functions for the i^{th} and j^{th} elements of the phase-space, i.e., the difference between the target and iteratively obtained values of (Φ^R, Φ^T) . Then, for each element of the phase-space the multi-objective optimization problem can be formulated as

$$\min_{(l, d_1, d_2) \in \mathbb{R}} \left[\epsilon_1^{i,j}(l, d_1, d_2), \epsilon_2^{i,j}(l, d_1, d_2) \right]. \quad (8)$$

Figures 2(a,b) show the resulting minimization values for each (Φ^R, Φ^T) combination considered, with a maximum discrepancy of 0.04% compared to targeted values. Figure 2(c) illustrates all the Pareto values obtained during the multi-objective optimization and displays in black the minima for each Pareto front.

3. LENS DESIGN

In order to design a lens that can behave as an ideal scatterer in both reflection and transmission directions, the latter must display a phase distribution coefficient at the surface, $\xi(x, y)$, such that the spatial Fourier transform of said distribution approximates a flat distribution. There are many number theoretic sequences that can help design such phase distribution, such as the maximum length or quadratic residue sequences [12]. Here, the quadratic residue (QR) sequence will be used. A 2D QR-sequence composed of $(x, y)N \times M$ elements can be expressed as

$$s_{n,m} = n^2 + m^2 \bmod N, \quad (9)$$

where n and m are integers and indices of the sequence for the n^{th} and m^{th} element in the x and y directions, respectively. Diffusers based on QR-sequences work at integer multiples of a design frequency, f_d , or wavelength, λ_d . In order to obtain the phase distribution of a 2D QR-sequence, we use the design equations of concert hall acoustic diffusers in which the depth $d_{n,m}$ of air above the n^{th} and m^{th} element of the diffuser (traditionally a

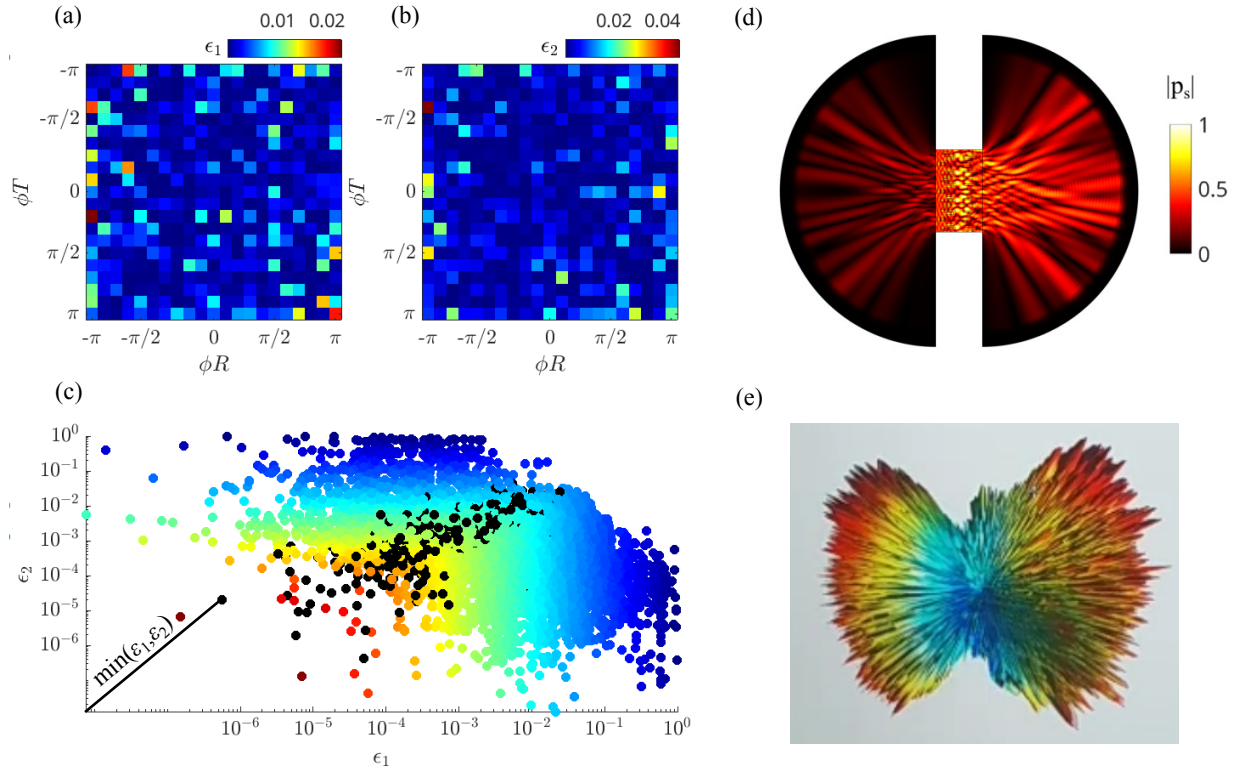


Figure 2. (a) Minimization minima for the multi-optimization phase-space (Φ^R, Φ^T) for reflection and (b) transmission. (c) Pareto front of the multi-objective optimization with minima for each i -th and j -th iteration (black). (d) Numerical scattered pressure field made by a 53×53 lens. (e) Experimental scattered pressure field made by a 53×53 lens repeated 3 times (see Fig. 1(a)).

quarter-wavelength resonator) is given as a function of the sequence profile which can be expressed as

$$d_{n,m} = \frac{s_n \lambda_d}{2N}. \quad (10)$$

Here, the design frequency is chosen as half of the working frequency of the lens, i.e., $1.1 \text{ MHz} / 2$.

The last step for designing the bi-directional lens remains to go over each element (n, m) of the lens which is related to the target QRD phase on both sides, and find the lengths (l, d_1, d_2) associated to the phase combination element $\Phi(i, j)$ in the phase-space matrix that is the closest of both reflected and transmitted phase values.

4. NUMERICAL & EXPERIMENTAL RESULTS

Figure 2(d) shows a (z, x) cross-section of the scattered pressure field on both sides of a lens with 53 constituting

blocks obtained numerically via Finite Element Method (FEM). The lens is embedded between two hemi-spherical water media with Perfectly Matched Layers (PML) and a plane wave of 1.1 MHz propagating from the left to the right. It can be observed that the scattered acoustic energy is being radiated quite omnidirectionally from both sides of the lens, albeit with a stronger intensity in the transmission direction than in reflection. This is due to the low impedance match between water and the polymer being used, which is quite convenient for many ultrasound applications where a great portion of sound must still go through the lens; the purpose here being to tune the directivity of the otherwise directional ultrasonic beam. However, the reflected portion of the impinging sound wave is also here scattered as evenly as the transmitted one thus preventing any unwanted specular reflections.

Figure 2(e) shows the 3D measured scattered field

made by a $3 \times (53 \times 53)$ lens in a water tank experiment (see Fig. 1(a)). A similar behaviour can be observed in the scattering pattern in both reflection and transmission where more acoustic energy is being transmitted compared to the reflected one, yet both scattered fields result in quite omnidirectional radiation patterns emerging from the lens at the centre. This illustrates a good agreement between theory and numerical simulations.

5. CONCLUSION

This work presents a bi-directional asymmetric diffusing lens for ultrasound applications where both sides can be encoded with different phase profiles for custom scattering patterns in both reflection and transmission. The phase profile encoding is made by discretizing the lens into a set of numerous constituting polymer blocks that affect the impinging wave with a certain phase shift induced by their varying length. The set of varying polymer lengths can be obtained using a multi-objective minimization algorithm which tries to obtain the closest match in all the possible reflected and transmitted phase values that could be ultimately used for the desired phase profiles.

Such work could be useful in situations where transmitted and reflected wavefields need to be controlled at the same time, such as a bi-directional diffusing lens emitting and receiving equally in and from all directions (equivalent of perfect optical diffusers in optics) or as a bi-directional beam directivity selector, e.g., focusing/collimating/decollimating beam switch. Such lens could also be used directly in reflection situations for minimizing unwanted reflections, e.g., reflections from surgical instruments during ultrasound-guided medical procedures.

6. REFERENCES

- [1] G. Kossoff, "Basic physics and imaging characteristics of ultrasound," *World journal of surgery*, vol. 24, pp. 134–42, 03 2000.
- [2] Y. Meng, Z. Shirzadi, B. MacIntosh, C. Heyn, G. Smith, I. Aubert, C. Hamani, S. Black, K. Hynynen, and N. Lipsman, "Blood-brain barrier opening in alzheimer's disease using mr-guided focused ultrasound," *Neurosurgery*, vol. 66, 09 2019.
- [3] B. Sigel, "A brief history of doppler ultrasound in the diagnosis of peripheral vascular disease," *Ultrasound in Medicine & Biology*, vol. 24, no. 2, pp. 169–176, 1998.
- [4] O. Demeulenaere, Z. Sandoval, P. Mateo, A. Dizeux, O. Villemain, R. Gallet, B. Ghaleh, T. Deffieux, C. Deméné, M. Tanter, C. Papadacci, and M. Pernot, "Coronary flow assessment using 3-dimensional ultrafast ultrasound localization microscopy," *JACC: Cardiovascular Imaging*, 2022.
- [5] S. Jiménez-Gambín, N. Jiménez, J. M. Benlloch, and F. Camarena, "Holograms to focus arbitrary ultrasonic fields through the skull," *Phys. Rev. Applied*, vol. 12, p. 014016, Jul 2019.
- [6] I. S. Elhelf, H. Albahar, U. Shah, A. Oto, E. Cressman, and M. Almekkawy, "High intensity focused ultrasound: The fundamentals, clinical applications and research trends," *Diagnostic and Interventional Imaging*, vol. 99, no. 6, pp. 349–359, 2018.
- [7] K. Melde, A. Mark, T. Qiu, and P. Fischer, "Holograms for acoustics," *Nature*, vol. 537, pp. 518–522, 09 2016.
- [8] G. Memoli, M. Caleap, M. Asakawa, D. Sahoo, B. Drinkwater, and S. Subramanian, "Metamaterial bricks and quantization of meta-surfaces," *Nature Communications*, vol. 8, p. 14608, 01 2017.
- [9] G. Allevato, J. Hinrichs, D. Großkurth, M. Rutsch, J. Adler, A. Jäger, M. Pesavento, and M. Kupnik, "3d imaging method for an air-coupled 40 khz ultrasound phased-array," 09 2019.
- [10] P. Kruijzinga, P. Meulen, A. Fedjajevs, F. Mastik, G. Springeling, N. Jong, J. Bosch, and G. Leus, "Compressive 3d ultrasound imaging using a single sensor," *Science Advances*, vol. 3, p. e1701423, 12 2017.
- [11] M. R. Schroeder, "Diffuse sound reflection by maximum length sequences," *The Journal of the Acoustical Society of America*, vol. 57, no. 1, pp. 149–150, 1975.
- [12] T. Cox and P. D'Antonio, "Schroeder diffusers: A review," *Building Acoustics*, vol. 10, no. 1, pp. 1–32, 2003.
- [13] N. Jiménez, O. Umnova, and J.-P. Groby, *Acoustic Waves in Periodic Structures, Metamaterials, and Porous Media*. Cham, Switzerland: Springer International Publishing, 2021.
- [14] T. D. Rossing, F. Dunn, W. M. Hartmann, D. M. Campbell, and N. H. Fletcher, *Springer Handbook of Acoustics*. Springer Publishing Company, Incorporated, 1st ed., 2007.